Transmission Line Distance Protection Under Current Transformer Saturation

Yuping Zheng, Tonghua Wu, Feng Hong, Gang Yao, Jimin Chai, and Zhinong Wei

***Abstract*—Conventional transmission line distance protection approaches are subject to malfunction under reverse fault-induced current transformer (CT) saturation for the typically employed breaker-and-a-half configuration. This paper addresses this issue by proposing a new distance protection approach that combines the blocking and unblocking criteria of distance protection based on the values of incomplete differential current, operation voltage, and current harmonic content. The proposed approach is verified by theoretical analysis, dynamic simulation testing, and field operation to ensure that the obtained distance protection is reliable and refrains from operating unnecessarily under reverse fault-induced CT saturation in the breaker-and-a-half configuration. Meanwhile, the proposed approach is demonstrated can operate reliably when forward faults occur or various reverse faults are converted to forward faults.**

***Index Terms*—Breaker-and-a-half configuration, current transformer (CT) saturation, distance protection, power frequency variation, operation voltage.**

I. Introduction

THE operation range and sensitivity of distance protection are not directly affected by the operation mode of an electric power transmission system. Therefore, distance protection can satisfy the requirements of modern power systems for rapid fault clearing and hence can be widely used in high-voltage transmission lines [1], [2]. However, the transmission characteristics of current transformers (CTs) are important factors that affect the dependability of distance protection, particularly under secondary current distortion during CT saturation [3].

According to the IEC 60255-121 standard [3], the effect of CT saturation on distance protection can be classified into two categories: dependability loss and security loss. A dependability loss corresponds to a saturation-induced decrease in the current amplitude and a phase shift, which reduces the actuation range and increases the actuation time of distance protection. A security loss corresponds to a distance protection malfunction that arises from a saturation-induced reverse current. Generally, in the case of a single CT connected to protection, distance protection will lose dependability with reduced possibility of malfunction owing to a decrease in the secondary current after CT saturation. Similar conclusions have been drawn in the literature [4], [5].

However, according to the IEEE Std C37.110 [6], in a ring or breaker-and-a-half configuration, the current used for line protection is the sum of the currents of two CTs. When the bus fails, a large ride-through current may flow through the CT. If the CT is saturated, the total current may present a large reverse current, and the distance protection will be at the risk of malfunction.

The problems associated with distance protection under CT saturation have been addressed in a number of studies. For example, the optimal selection of CTs at key locations in the transmission system has been verified to be effective for reducing or avoiding the effect of CT saturation on distance protection [6]. However, this complicates the implementation and application range of distance protection. Hence, these problems cannot be resolved completely by depending solely on the optimal selection of CT locations. Other studies have proposed the use of new types of CTs such as Rogowski coils or electromagnetic CTs to limit the effect of CT saturation on distance protection [7], [8]. However, these new types of CTs cannot be applied in a sufficiently extensive manner to address these problems owing to issues regarding stability and economic considerations. Furthermore, studies focusing on the malfunction of distance protection during CT saturation are rather limited, and most previous studies investigate the malfunction of differential protection during CT saturation, including some approaches such as the identification approach of saturated waveforms [9]-[13] and the compensation approach for saturation current [14]-[17]. In addition, an approach employing directional elements has been proposed to avoid malfunction [18]. However, the operation conditions under which this method is applicable are limited, and malfunctions can still occur in special cases. Moreover, distance protection malfunctions in high-voltage transmission lines significantly affect the power grid, particularly in the ring or breaker-and-a-half configuration, and the risk of malfunction during

Manuscript received: October 12, 2019; accepted: July 7, 2020. Date of CrossCheck: July 7, 2020. Date of online publication: November 20, 2020.

This work was supported by Science and Technology Program of State Grid Corporation of China "Research on Fault Coupling Characteristics and New Protection Principle of AC/DC Hybrid Power Grid".

Y. Zheng, T. Wu (corresponding author), J. Chai, and Z. Wei are with the College of Energy and Electrical Engineering, Hohai University, Nanjing 210098, China, Y. Zheng and T. Wu are also with State Key Laboratory of Smart Grid Protection and Control, NARI Group Corporation, Nanjing 211106, China, and J. Chai is also with Changzhou Institute of Technology, Changzhou 213032, China (e-mail: zhengyuping@sgepri.sgcc.com.cn; wutonghua@sgepri.sgcc.com.cn; chaijm@czu.cn; wzn_nj@263.net).

F. Hong and G. Yao are with State Key Laboratory of Smart Grid Protection and Control, NARI Group Corporation, Nanjing 211106, China (e-mail: hongfeng@ sgepri.sgcc.com.cn; yaogang@ sgepri.sgcc.com.cn).

DOI: 10.35833/MPCE.2019.000095

reverse fault-induced CT saturation events is high. Accordingly, it is essential to analyze the causes of malfunctions in distance protection during CT saturation for developing reliable preventative approaches.

Herein, the mechanism of distance protection malfunction during reverse fault-induced CT saturation is analyzed for the breaker-and-a-half configuration as an example. Accordingly, a new distance protection approach is proposed that combines the blocking and unblocking criteria of distance protection based on the criteria of incomplete differential current, operation voltage, and current harmonic content. The proposed approach is validated by theoretical analysis, dynamic simulation testing, and field operation to ensure that the obtained distance protection is reliable and can be implemented appropriately during reverse fault-induced CT saturation in the ring or breaker-and-a-half configuration. Meanwhile, the proposed approach is demonstrated can operate reliably when forward faults occur or various reverse faults are converted to forward faults owing to the subsidence of CT saturation.

II. Analysis of Distance Protection Malfunction

The mho characteristic is one of the most typically used characteristics in distance protection [3]. In this study, we perform an analysis based on an example of mho distance protection [19] of positive-sequence voltage polarization. Based on the phase-comparison principle, the operation equation is expressed as:

$$90° < \arg(\dot{U}_{OP}/\dot{U}_P) < 270° \tag{1}$$

where $\dot{U}_{OP} = \dot{U}_m - \dot{I}_m Z_{set}$ is the operation voltage, and Z_{set} is the setting value of distance protection, $\dot{U}_m$ and $\dot{I}_m$ are the respective voltage and current obtained by the protection device, respectively; and $\dot{U}_P = \dot{U}_{m1}$ is the polarization voltage, and $\dot{U}_{m1}$ is the positive-sequence voltage component at the protection device.

According to an example of a substation system shown in Fig. 1, the current $\dot{I}_{ml}$ on the protected line L_1 is the sum of the primary currents $\dot{I}_{m1}$ from CT1 and $\dot{I}_{m2}$ from CT2.

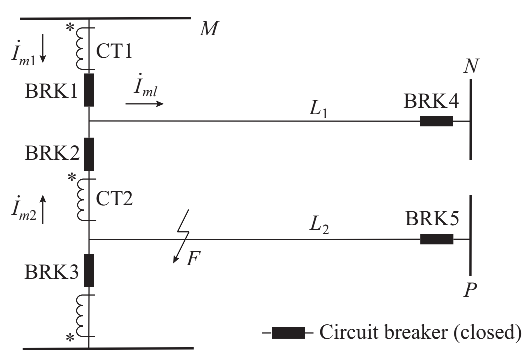

Fig. 1. An example of a substation system with breaker-and-a-half configuration.

According to the characteristics of CT transmission, $\dot{I}_{m1}$ and $\dot{I}_{m2}$ can be expressed as [3]:

$$\dot{I}'_{m1} = \dot{k}_1 \dot{I}_{m1} \tag{2}$$

$$\dot{I}'_{m2} = \dot{k}_2 \dot{I}_{m2} \tag{3}$$

where $\dot{I}'_{m1}$ and $\dot{I}'_{m2}$ are the secondary currents from CT1 and CT2, respectively; and $\dot{k}_1 = A\mathrm{e}^{\phi}$. A and ϕ are the changes in the amplitude and angular difference generated during transmission, respectively. The definition of $\dot{k}_2$ is similar. A virtual CT that outputs the secondary total current can be constructed, and according to (2) and (3), the transmission characteristic of CT can be expressed as:

$$\dot{k} = \frac{\dot{I}'_{sum}}{\dot{I}_l} = \frac{\dot{I}'_{m1} + \dot{I}'_{m2}}{\dot{I}_{m1} + \dot{I}_{m2}} = \frac{\dot{k}_1 \dot{I}_{m1} + \dot{k}_2 \dot{I}_{m2}}{\dot{I}_{m1} + \dot{I}_{m2}} \tag{4}$$

where $\dot{I}_l$ is the primary current flowing through the line; and $\dot{I}'_{sum}$ is the total current flowing to the protection device. For simplicity, the CT1 and CT2 ratios are assumed to be 1. Therefore, $\dot{k}_1 = \dot{k}_2 = 1$ during a normal CT transmission.

The equivalent system obtained when a fault occurs at point F of line L_2 in Fig. 1 is shown in Fig. 2, where $\dot{E}_S$ is the sending-end electromotive force; $\dot{E}_R$ is the receiving-end electromotive force; $\dot{I}_F$ is the fault current flowing from point F to point K; Z_K is the equivalent impedance from point M to point K; and Z_R is the equivalent impedance of the protection forward direction.

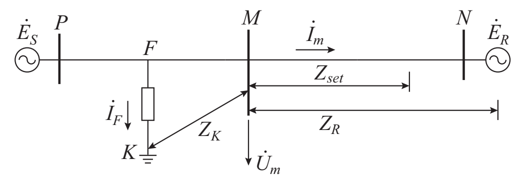

Fig. 2. Equivalent system with reverse fault at point F in Fig. 1.

The parameters in Fig. 2 are used to express the operation voltage $\dot{U}_{OP}$ and polarization voltage $\dot{U}_P$ as:

$$\dot{U}_{OP} = \dot{U}_m - \dot{I}'_l Z_{set} = \dot{I}_l Z_m - \dot{k}\dot{I}_l Z_{set} = \dot{I}_l (Z_m - \dot{k} Z_{set}) \tag{5}$$

$$\begin{aligned}\dot{U}_P = \dot{U}_{m1} &= \dot{E}_R + \dot{I}_{l1} Z_R = -\dot{I}_l (Z_R - Z_m) + \dot{I}_{l1} Z_R = \\ &\dot{I}_l [Z_m - Z_R (1 - \dot{I}_{l1}/\dot{I}_l)] = \dot{I}_l (Z_m - k' Z_R)\end{aligned} \tag{6}$$

where Z_m is the resistance between the protection device and the short-circuit point; $\dot{I}_{l1}$ is the positive-sequence component of $\dot{I}_l$; and $k' = 1 - \dot{I}_{l1}/\dot{I}_l$, which is related to the fault type and system parameter. For example, with a single-phase earth fault, $k' = 0.75 - 0.87$; with a phase-phase fault, $k' = 0.5$; and with a three-phase fault, $k' = 0$.

Substituting (5) and (6) into (1) yields

$$90° < \arg \frac{Z_m - \dot{k} Z_{set}}{Z_m - k' Z_R} < 270° \tag{7}$$

The operation characteristic corresponding to (7) is a circle with end points of $\dot{k} Z_{set}$ and $k' Z_R$ as the diameter. During the normal transmission of CT1 and CT2, $\dot{k} = 1$. This condition is illustrated in Fig. 3(a), where the action circle is removed from the origin toward quadrant I. The reverse fault measurement impedance $-Z_k$ generally falls in quadrant III, and hence the relay exhibits good directionality. By contrast, when CT1 is under normal transmission and CT2 is under severe saturation, $\dot{k}_1 = 1$, whereas the amplitude of $\dot{k}_2$ is reduced and becomes zero [6]. This condition is illustrated in Fig. 3(b), where $\dot{k} = \dot{I}'_{m1}/\dot{I}_l$ owing to the opposite directions of $\dot{I}'_{m1}$ and $\dot{I}_l$, and the action circle corresponding to (7) shifts to quadrant III. Therefore, distance protection may malfunction when a short-circuit fault occurs at the far-end point or the opposite bus.

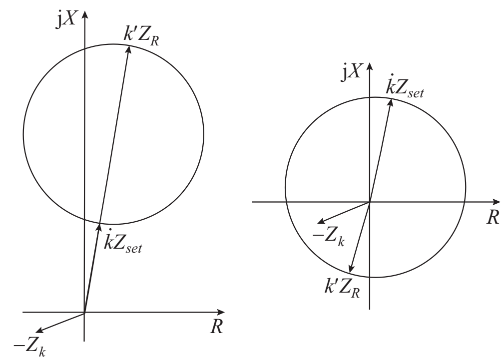

Fig. 3. Mho action circle with positive-sequence voltage polarization. (a) Transmission of both CT1 and CT2 is normal. (b) CT2 is saturated.

The system illustrated in Fig. 1 presents a special operation condition, denoted as operation condition 1, when BRK4 is disconnected with a reverse fault at point F so that the same current flows through CT1 and CT2, and $\dot{I}_l$ is zero. The condition where CT2 is severely saturated is illustrated in Fig. 4, where the total current $\dot{I}'_{sum}$ from the CT output presents a consistent positive-direction characteristic with respect to $\dot{I}'_{m1}$. Subsequently, $\dot{k}$ is in quadrant III, and the amplitude approaches infinity. Herein, the action circle corresponding to (7) extends infinitely to quadrant III, and the possibility of a reverse-fault-induced malfunction arises.

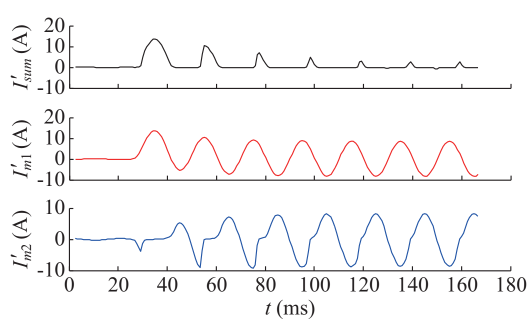

Fig. 4. CT2 saturation with reverse fault under operation condition 1.

Fault currents flowing through the branch CT may differ significantly, thereby resulting in the saturation of one of the CTs. For the fault illustrated in Fig. 1 and analyzed above, the fault currents from bus M and line L_1 flowing through CT2 are easily saturated. Moreover, the directional characteristics of the total current are affected by CT2 saturation. Namely, the total current moves gradually in the forward direction as the extent of CT2 saturation increases, thereby increasing the probability of distance protection malfunction. Furthermore, a similar situation occurs with the fault at point F_b, as shown in Fig. 5(b). Hence, both the fault position and CT saturation extent are the factors that affect the distance protection malfunction.

Additional short-circuit states are illustrated in Fig. 5(a) and (b), which represent a fault at the near-end point F_a along the forward direction of the line and a fault at point F_b on the reverse bus, respectively. Figure 5(a) shows that, when the fault occurs at point F_a, variations $\Delta\dot{I}_{m1}$ and $\Delta\dot{I}_{m2}$ of the current flowing through CT1 and CT2 are reversed, i.e., they are in the same direction. Figure 5(b) shows that when the fault occurs at point F_b, $\Delta\dot{I}_{m1}$ is forward and $\Delta\dot{I}_{m2}$ is reverse, i.e., the two are in opposite directions. These two short-circuit states are analyzed in much greater detail in the following section. However, the fault at point F_b shown in Fig. 5(b) is similar to the fault illustrated in Fig. 1 and that analyzed previously.

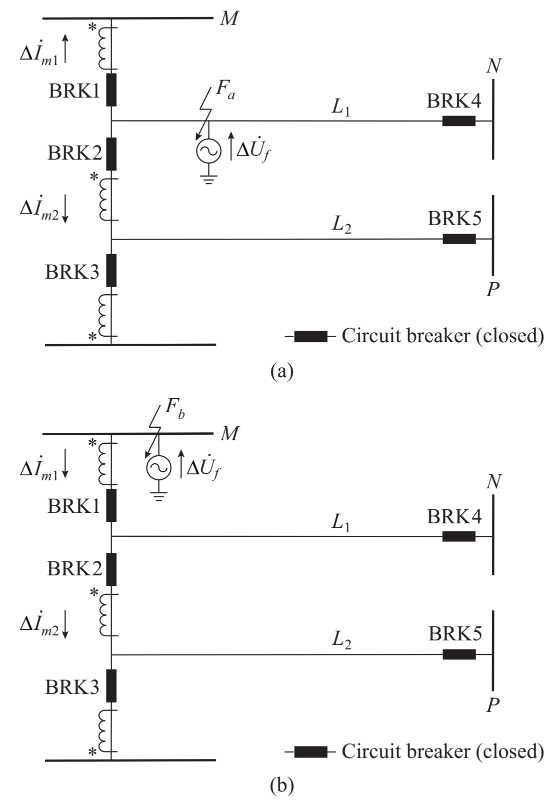

Fig. 5. Schematic diagrams for illustrating additional short-circuit states of substation system with breaker-and-a-half configuration shown in Fig. 1. (a) Forward short-circuit fault. (b) Reverse short-circuit fault.

To summarize, distance protection is at the risk of malfunction in the case of reverse-fault-induced CT saturation in the breaker-and-a-half configuration and will malfunction under particular operation modes. In addition, the fault location and extent of CT saturation are the factors affecting the distance protection malfunction.

III. Identification Method for CT Saturation for Distance Protection

A. Incomplete Differential Criteria

The fault current direction characteristics of the short-circuit states illustrated in Fig. 5(a) and (b) enable the formulation of incomplete differential criteria for conducting distance protection. Among the distance protection criteria, the blocking criterion and the unblocking criterion are expressed as (8) and (9), respectively.

$$\begin{cases}\Delta I_{cd} \le k_{res}\Delta I_{zd} \\ \Delta I_{zd} > I_{set,zd}\end{cases} \tag{8}$$

$$\begin{cases}\Delta I_{cd} > k_{res}\Delta I_{zd} \\ \Delta I_{zd} > I_{set,zd}\end{cases} \tag{9}$$

where $\Delta I_{cd} = \left|\Delta \dot{I}_{m1} + \Delta \dot{I}_{m2}\right|$ is the incomplete differential current; $\Delta I_{zd} = \left|\Delta \dot{I}_{m1} - \Delta \dot{I}_{m2}\right|$ is the incomplete restraint current; k_{res} is the differential restraint coefficient, which is generally set as 1.1; and $I_{set,zd}$ is the restraint current threshold, which is set to avoid the effect of system disturbances on the criterion and causes the criterion to exhibit great sensitivity for the near-end metallic fault and not subject to false blocking during the far-end reverse line fault.

The values of $\Delta \dot{I}_{m1}$ and $\Delta \dot{I}_{m2}$ are obtained using the short data window algorithm [20], [21]. The criteria can identify the fault direction during CT saturation [3] and can implement distance protection for a forward fault while blocking distance protection for a reverse fault. In the far-end reverse line fault (Fig. 5(b)), the blocking criterion is not subject to false blocking. In addition, the amplitudes of $\Delta \dot{I}_{m1}$ and $\Delta \dot{I}_{m2}$ are high for the near-end metallic fault, and the directional characteristics are conspicuous. Hence, the criteria exhibit greater sensitivity. However, a small fault current arising under fault conditions such as a far-end fault or near-end fault with transition resistance may induce CT saturation under residual CT magnetism. Under these conditions, the directional characteristics of $\Delta \dot{I}_{m1}$ and $\Delta \dot{I}_{m2}$ are not conspicuous and hence the criteria may be invalid. This can be analyzed based on the system illustrated in Fig. 6, where the two transmission lines from bus M are installed on the same tower. When BRK3 is open, which is defined as operation condition 2, a short-circuit fault occurs at the end of the line or on the bus N, and $\Delta \dot{I}_{m2}$ may be extremely small. At this point, $\Delta I_{cd} \approx \Delta I_{zd}$, and the blocking criterion operates to halt the implementation of distance protection. These problems are addressed by the proposed operation voltage criteria.

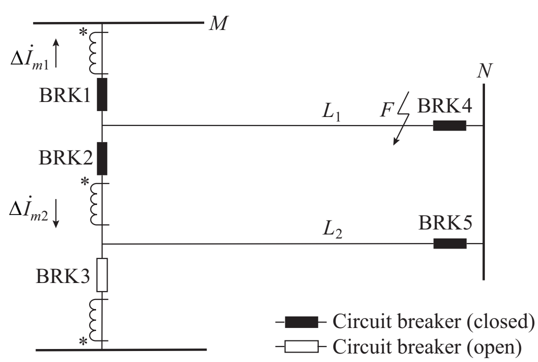

Fig. 6. Operation condition 2: double-circuit lines on the same tower with BRK3 open.

B. Operation Voltage Criteria

The operation voltage variation $\Delta \dot{U}_{op}$ is defined as:

$$\Delta \dot{U}_{op} = \Delta \dot{U}_m - \Delta \dot{I}_m Z_L \tag{10}$$

where Z_L is the impedance of the entire transmission line; and $\Delta \dot{U}_m$ and $\Delta \dot{I}_m$ are the voltage and current variations at the protection device, respectively. This can be defined in cases of forward and reverse faults as follows.

For the forward fault,

$$\Delta \dot{U}_m = -\Delta \dot{I}_m Z_S \tag{11}$$

where Z_S is the equivalent positive-sequence impedance of the power system behind the protection device. Substituting (11) into (10), we can obtain

$$\Delta \dot{U}_{op} = -\Delta \dot{I}_m (Z_S + Z_{set}) \tag{12}$$

The voltage variation at fault point F is defined as:

$$\Delta \dot{U}_f = \Delta \dot{I}_m (Z_S + Z_F) \tag{13}$$

where Z_F is the positive-sequence impedance from the short-circuit point F to the protection device. The forward fault is illustrated by the potential diagram of the voltage variation, as shown in Fig. 7(a). Accordingly, the condition $\left|\Delta \dot{U}_{op}\right| > \left|\Delta \dot{U}_m\right|$ must hold along the entire transmission line during a short circuit in the forward direction.

For a reverse fault,

$$\Delta \dot{U}_m = \Delta \dot{I}_m Z_R \tag{14}$$

where Z_R is the equivalent positive-sequence impedance of the protection forward direction. Substituting (14) into (10), we can obtain

$$\Delta \dot{U}_{op} = \Delta \dot{I}_m (Z_R - Z_L) \tag{15}$$

The voltage variation at fault point F is expressed as:

$$\Delta \dot{U}_f = -\Delta \dot{I}_m (Z_R + Z_F) \tag{16}$$

The reverse fault is illustrated by the potential diagram of the voltage variation, as shown in Fig. 7(b). Accordingly, the condition $\left|\Delta \dot{U}_{op}\right| < \left|\Delta \dot{U}_m\right|$ must be met during a reverse short circuit.

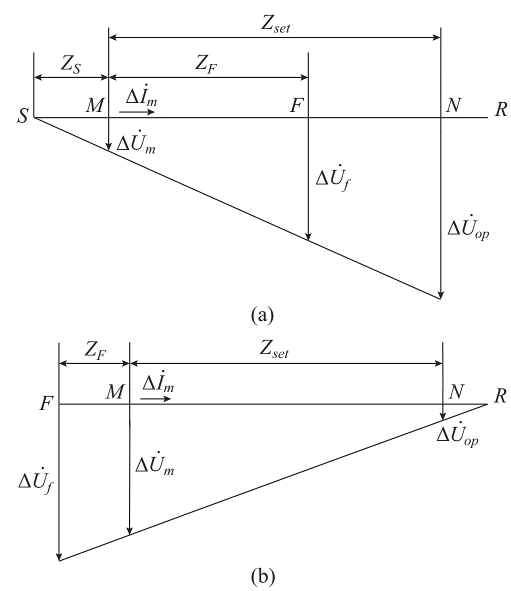

Fig. 7. Distribution diagram for reverse fault voltage variation. (a) Forward fault. (b) Reverse fault.

Based on the above analysis, different relationships involving $\Delta \dot{U}_{op}$ and $\Delta \dot{U}_m$ are employed to set unblocking and blocking criteria of the operation voltage during positive and reverse faults, which are expressed as (17) and (18), respectively.

$$\begin{cases} \left|\Delta \dot{U}_{op}\right| > k\left|\Delta \dot{U}_m\right| \\ \left|\Delta \dot{U}_m\right| > U_{set,dif} \end{cases} \tag{17}$$

$$\begin{cases} \left|\Delta \dot{U}_{op}\right| < k\left|\Delta \dot{U}_m\right| \\ \left|\Delta \dot{U}_m\right| > U_{set,dif} \end{cases} \tag{18}$$

where $U_{set,dif}$ is the voltage threshold value; and k is the restraint coefficient, which is generally set as 1.1, and ensures that the blocking criterion is reliable. Similar to (8), the threshold value $U_{set,dif}$ is also set to reduce the effect of disturbance in the system on the criterion. The values of $\Delta \dot{U}_m$ and $\Delta \dot{I}_m$ are obtained using the short data window algorithm [20], [21]. Under normal operation conditions, the criteria can identify the fault direction during CT saturation [3] and then implement distance protection for a forward fault while blocking distance protection for a reverse fault. Details regarding the application of the operation voltage criteria under the two operation conditions are provided as follows.

Under operation condition 1, the total current obtained by the protection is zero during a reverse bus fault. At this time, $\left|\Delta \dot{U}_{op}\right| = \left|\Delta \dot{U}_m\right|$, and the blocking criterion of (18) is invalid. During the forward fault, $\left|\Delta \dot{U}_{op}\right|$ is significantly greater than $\left|\Delta \dot{U}_m\right|$; hence, the value of k cannot impair the judgment of the unblocking criterion. Under this operation condition, the incomplete differential blocking criterion operates correctly and exhibits greater sensitivity than the operation voltage blocking criterion.

Under operation condition 2, the incomplete differential criterion is invalid during a fault at the remote end of the line. However, the operation voltage unblocking criterion operates correctly and exhibits greater sensitivity than the incomplete differential unblocking criterion.

The above analysis demonstrates the necessity of utilizing both the incomplete differential and operation voltage criteria to address special conditions where a single set of criteria is not applicable.

C. Logic Coordination Between Incomplete Differential and Operation Voltage Criteria

The action conditions of the incomplete differential and operation voltage criteria at various fault points under different system conditions are shown in Table I, where P_1, P_2, and P_3 denote the fault points at the near-end line, far-end line, and opposite bus, respectively.

TABLE I
ACTION CONDITION OF INCOMPLETE DIFFERENTIAL AND OPERATION VOLTAGE CRITERIA

Condition	Fault point	Incomplete differential blocking criterion	Incomplete differential unblocking criterion	Operation voltage blocking criterion	Operation voltage unblocking criterion
Condition 1	P_1	Action	No action	Action	No action
	P_2	No action	Action	Action	No action
	P_3	No action	Action	Action	No action
Condition 2	P_1	Action	No action	Action	No action
	P_2	No action	Action	No action	Action
	P_3	Action	No action	No action	Action
General	P_1	Action	No action	Action	No action
	P_2	No action	Action	No action	Action
	P_3	No action	Action	No action	Action

The following conclusions can be obtained from Table I.

1) Under operation condition 1, the operation voltage blocking criterion is always activated regardless of the fault type, whereas the operation voltage unblocking criterion is never activated, and the incomplete differential action criteria are activated normally.

2) Under operation condition 2, the incomplete differential blocking criterion is activated in the fault at P_3, whereas the incomplete differential unblocking criterion is not activated, and the operation voltage criteria are activated normally.

3) Under general operation conditions, both the incomplete differential and operation voltage criteria are activated normally.

Accordingly, valid distance protection blocking actions are assured by applying an "and" logic to the criteria of the incomplete differential blocking and the operation voltage blocking, whereas valid distance protection unblocking actions are assured by applying an "or" logic to the criteria of the incomplete differential unblocking and operation voltage unblocking. Hence, the criteria provide a strict account of the fault direction under all operation conditions. The criteria are activated according to the characteristics of the linear transmission area of the CT prior to its saturation. Consequently, a logical interlock between the blocking and unblocking criteria is used to avoid the effect of current distortion on criteria decisions after CT saturation, as shown in Fig. 8, and the continuity of the criteria can be maintained during CT saturation.

D. Criteria for Current Harmonic Content Unblocking

When a reverse fault is converted to a forward fault, the distance protection blocking criteria act first and maintain the action, resulting in a failure to unblock distance protection after conversion to the forward fault. This problem is addressed in the present study by establishing unblocking criteria based on the current harmonic content.

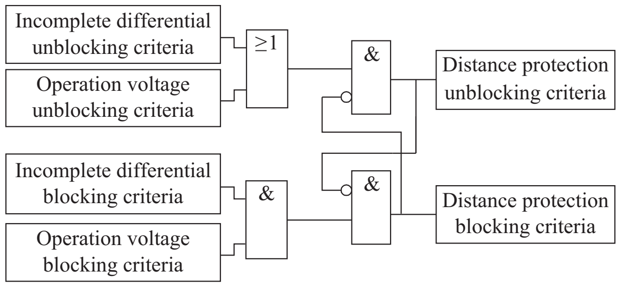

Fig. 8. Logic diagram for applying distance protection blocking and unblocking criteria.

The high second harmonic content of the output current is the key feature of CT saturation [19], [22], [23]. Accordingly, CT saturation can be assumed to be relieved when the second harmonic content of the output current is less than a threshold value, enabling distance protection to be unblocked. The proposed current harmonic content unblocking criteria are expressed as:

$$\begin{cases} I_{m,h2} < k_H I_m \\ I_{m1,h2} < k_H I_{m1} \\ I_{m2,h2} < k_H I_{m2} \end{cases} \tag{19}$$

where $I_{m,h2}$, $I_{m1,h2}$, and $I_{m2,h2}$ are the secondary harmonic contents of the total current, side circuit breaker current, and middle circuit breaker current, respectively; I_m, I_{m1}, and I_{m2} are the total current, side circuit breaker current, and middle circuit breaker current, respectively; and k_H is the harmonic content ratio coefficient, which is set as 0.15 based on the literature [22]-[24] and a large number of simulation tests.

During a reverse fault, distance protection is blocked, and the output current is monitored according to the criteria in (19) simultaneously. If CT saturation is relieved and the reverse fault is converted to a forward fault, the harmonic contents will be less than the threshold values, and distance protection will be unblocked. During forward-fault-induced CT saturation, the action characteristics of distance protection are affected by distortions in the current, and the protection trip time will be extended or the protection range will be reduced [4]. Meanwhile, the action characteristics cannot be restored until CT saturation has subsided to a certain extent or completely relieved. Therefore, the full-cycle Fourier algorithm is used to implement a criterion that has a short time delay, and the criterion can be unblocked in time with limited effect on the action characteristics of the distance protection.

IV. Simulation Analysis

A. Simulation System Parameter

Figure 9 presents the dual-circuit simulation model built in the Real Time Digital Simulator (RTDS) and employed for analysis. It is a typical model operating at 500 kV, where the same tower adopts the breaker-and-a-half configuration at one side and the dual-bus configuration at the other side. Internal fault points F_1-F_3 and external fault points F_4 and F_5 are established in the model to simulate various fault types. The system impedance and line parameters are listed in Table II.

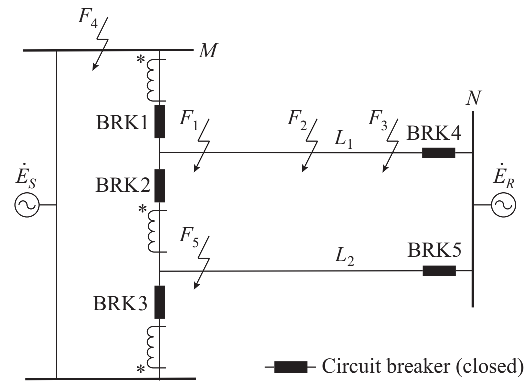

Fig. 9. RTDS simulation model.

TABLE II
System Impedance and Line Parameters of RTDS Simulation Model

Parameter	Value
Positive-sequence resistance (Ω/km)	0.028
Positive-sequence inductive reactance (Ω/km)	0.275
Positive-sequence capacitive reactance in parallel (Ω·km)	0.225
Zero-sequence resistance (Ω/km)	0.094
Zero-sequence inductive reactance (Ω/km)	0.674
Positive-sequence capacitive reactance in parallel (Ω·km)	0.313
Line length (km)	100
System equivalent impedance at bus M (Ω)	10∠85°
System equivalent impedance at bus N (Ω)	20∠85°

Two protection devices, denoted as A and B, are employed in the simulations at the M side of line L_1. Device A is developed based on the proposed method, and device B is developed using the conventional distance protection strategy. Device A measures the respective output currents of CT1 and CT2, whereas device B measures the total current. Both devices comprise two-stage distance protections based on the mho relay, which is defined in (1). The value of Z_{set} of distance relay zone I is 22.11 Ω, whereas it is set to be 33.16 Ω for the distance relay zone II, and the time delay is set to be 0.5 s.

B. Simulation Result

Dynamic simulations are conducted to verify the performance of the protection devices with forward and reverse metallic faults and different operation modes. The simulation results are listed in Table III. The results indicate that both devices A and B provide consistent operation characteristics of distance protection under general operation conditions as well as forward and reverse faults. Hence, the proposed approach does not affect the original operation characteristics of distance protection.

The fault recording results of device A in a fault at F_1 are shown in Fig. 10(a) to illustrate the criterion features obtained during a forward fault. After the fault occurs, the criteria of the incomplete differential unblocking and operation voltage unblocking are satisfied rapidly, and distance protection is unblocked. Similarly, the fault recording results of device A in a fault at F_5 are shown in Fig. 10(b) to illustrate the criterion features obtained during a reverse fault. After the fault occurs, the criteria of the incomplete differential blocking and operation voltage blocking are satisfied rapidly, and distance protection is blocked.

TABLE III
PERFORMANCE OF PROTECTION DEVICE UNDER DIFFERENT OPERATION MODES AND FAULTS

Mode	Fault point	Device A	Device B
Both strong	F_1	Distance relay zone I (12 ms)	Distance relay zone I (12 ms)
Both strong	F_2	Distance relay zone I (21 ms)	Distance relay zone I (21 ms)
Both strong	F_4	No action	No action
E_S strong, E_R weak	F_1	Distance relay zone I (10 ms)	Distance relay zone I (10 ms)
E_S strong, E_R weak	F_3	Distance relay zone II (521 ms)	Distance relay zone II (521 ms)
E_S strong, E_R weak	F_5	No action	No action

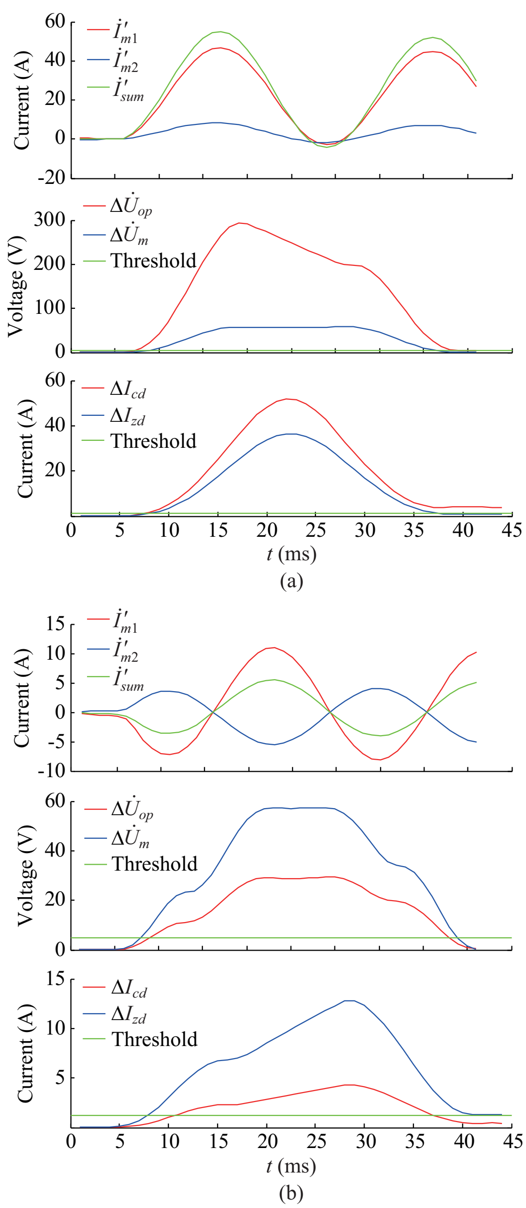

Fig. 10. Criterion features during forward and reverse faults. (a) Forward fault. (b) Reverse fault.

The dynamic simulation results obtained in transfer faults are listed in Table IV. The results indicate that both devices A and B provide consistent operation characteristics of distance protection. Furthermore, the results verify the feasibility of the current harmonic content unblocking criteria, which exhibit action features similar to those of the conventional method.

TABLE IV
ACTION OF PROTECTION DEVICE IN TRANSFER FAULT

Fault	Convert time (ms)	Device A	Device B
F_1 A-phase, F_4 B-phase	10	Distance relay zone I (12 ms), A-phase trip	Distance relay zone I (12 ms), A-phase trip
F_1 A-phase, F_4 A-phase	10	Distance relay zone I (12 ms), A-phase trip	Distance relay zone I (12 ms), A-phase trip
F_4 A-phase, F_1 B-phase	10	Distance relay zone I (22 ms), B-phase trip	Distance relay zone I (22 ms), B-phase trip
F_4 A-phase, F_1 A-phase	10	Distance relay zone I (22 ms), A-phase trip	Distance relay zone I (22 ms), A-phase trip
F_4 A-phase, CT1 saturation, F_1 A-phase	10	Distance relay zone I (25 ms), A-phase trip	Distance relay zone I (22 ms), A-phase trip

Dynamic simulations are conducted for reverse single-phase metallic ground faults and a fault through transition resistance at F_4 under different saturation degrees of CT1 and CT2. The respective actions of protection devices A and B are listed in Table V. The results indicate that device A can reliably block distance protection under the reverse fault-induced CT saturation when the saturation time is greater than or equal to 2 ms. By contrast, device B is subject to malfunction. Moreover, the blocking criteria of device A still have a greater sensitivity compared with the single blocking criterion of device B in the case of involving a fault through transition resistance. Additionally, the criteria provide a smaller fault current as well as reliable distance protection blocking.

TABLE V
PROTECTION ACTION OF REVERSE FAULT AT F_4

Fault type	Saturated CT	Saturation time (ms)	Device A	Device B
Metallic	CT1	1.5	Action	Action
	CT1	2.0	No action	Action
	CT1	2.5	No action	Action
	CT1	5.0	No action	Action
	CT2	2.0	No action	No action
	CT2	5.0	No action	No action
Through transition resistance	CT1	1.5	Action	Action
	CT1	2.0	No action	Action
	CT1	2.5	No action	Action
	CT1	5.0	No action	Action
	CT2	2.0	No action	No action

The fault recording results of device A in a fault at F_4 when CT1 is saturated are shown in Fig. 11. Therefore, the criteria of the incomplete differential blocking and operation voltage blocking are satisfied rapidly in the CT linear transmission region after the fault, and the distance protection is blocked.

Subsequently, the criteria of the operation voltage unblocking and incomplete differential unblocking are satisfied after entering the CT saturation region. However, the distance protection blocking criterion blocks the unblocking criterion, and the blocking status of the distance protection is maintained.

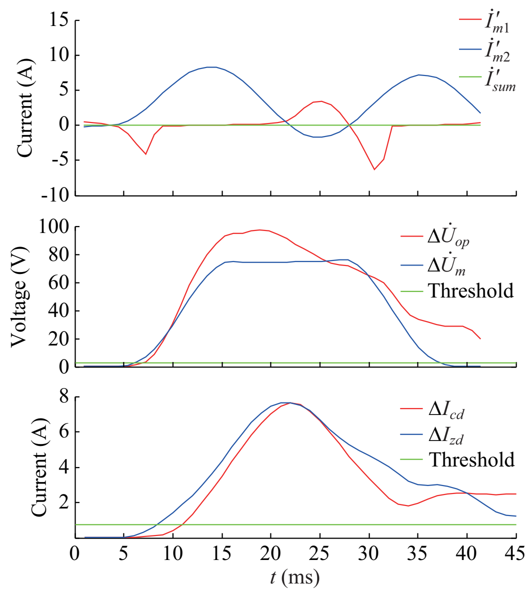

Fig. 11. Criterion feature in case of reverse fault and CT saturation.

In operation condition 1 for various operation modes, the single-phase grounding fault at F_3 occurs again.

The dynamic simulation results of a single-phase grounding fault at F_3 obtained under operation condition 1 combined with various modes at the two terminals are listed in Table VI. In addition, the actions of protection devices A and B obtained during simulations under operation condition 2 with a reverse single-phase grounding fault at F_5 are listed in Table VII for different saturation degrees of CT1 and CT2. The simulation results obtained under the two operation conditions demonstrate that device A does not fail to implement distance protection in the forward fault condition, and that it refrains from implementing distance protection unnecessarily under the reverse fault and CT saturation conditions. Meanwhile, device B is subject to malfunction. Hence, these results verify that the combination of the incomplete differential and operation voltage criteria addresses the problems associated with single-criterion approaches under special operation conditions. In addition, the correct criterion action is ensured under all operation conditions.

TABLE VI
PROTECTION ACTION OF FORWARD FAULT AT F_3

Condition	Device A	Device B
Both strong	Distance relay zone II (511 ms)	Distance relay zone II (512 ms)
Both weak	Distance relay zone II (512 ms)	Distance relay zone II (513 ms)
$\dot{E}_S$ strong, $\dot{E}_R$ weak	Distance relay zone II (512 ms)	Distance relay zone II (512 ms)
$\dot{E}_S$ weak, $\dot{E}_R$ strong	Distance relay zone II (512 ms)	Distance relay zone II (511 ms)

TABLE VII
PROTECTION ACTION OF EXTERNAL FAULT AT F_5

Saturated CT	Saturation time (ms)	Device A	Device B
CT1	2	No action	No action
CT1	5	No action	No action
CT2	2	No action	Action
CT2	5	No action	Action

Over 10000 protection devices based on the proposed approach have been used in power grids of various voltage levels in China, and all of the field protection devices are operating as intended.

V. CONCLUSION

This paper addresses the tendency of conventional transmission line distance protection approaches to malfunction under reverse fault-induced CT saturation by proposing a new distance protection approach. The approach combines the criteria of distance protection blocking and unblocking based on the criteria of incomplete differential current, operation voltage, and current harmonic content. The mechanism of distance protection malfunction during reverse fault-induced CT saturation is analyzed for the breaker-and-a-half configuration as an example. The results of dynamic simulation testing and field operation verify that the proposed approach guarantees reliable distance protection and the intended operation during forward faults and reverse fault-induced CT saturation that lasts longer than 2 ms. In general, the proposed approach does not affect the accuracy and speed of distance protection. Moreover, the application of current harmonic content criteria enables the implementation of distance protection after a reverse fault is converted to a forward fault. Consequently, the reliability of distance protection is improved, and a higher practical engineering value is obtained. Ring or breaker-and-a-half configurations are typically used in domestic and foreign high-voltage power grids; hence, the promotion and application of the proposed approach will improve the reliability of power transmission line protection and enhance the safe operation of power grids.

REFERENCES

[1] Z. Li, X. Lin, H. Weng *et al.*, "Efforts on improving the performance of superimposed-based distance protection," *IEEE Transactions on Power Delivery*, vol. 27, no. 1, pp. 186-194, Jan. 2012.

[2] K. G. Firouzjah, "Distribution network expansion based on the optimized protective distance of surge arresters," *IEEE Transactions on Power Delivery*, vol. 33, no. 4, pp. 1735-1743. Jan. 2018,

[3] *IEEE Guide for the Application of Current Transformers Used for Protective Relaying Purposes*, IEEE Std C37.110TM-2007, 2007.

[4] *Measuring Relays and Protection Equipment – Part 121: Functional Requirements for Distance Protection*, IEC 60255-121-2014, 2014.

[5] K. Wannous and P. Toman, "The impact of current transformer saturation on the distance protection," in *Proceedings of 17th International Scientific Conference on Electronic Power Engineering (EPE)*, Prague, Czech Republic, May 2016, pp. 257-261.

[6] J. Mooney, "Distance element performance under conditions of CT saturation," in *Proceedings of 61st Annual Conference for Protective Relay Engineers*, College Station, USA, Apr. 2008, pp. 1-9.

[7] A. N. Sarwade, P. K. Katti, and J. G. Ghodekar, "Enhancement of digital distance protection scheme with novel transducer," in *Proceedings of International Conference on Intelligent Computing and Application,*

Advances in Intelligent Systems and Computing, Singapore: Springer Nature, 2018, pp. 287-297.
[8] Q. Chen, H. Hou, D. You *et al*., "Research on improvements of using electronic current transformer on distance protection," in *Proceedings of 42nd International University Power Engineering Conference*, Brighton, UK, Oct. 2007, pp. 267-272.
[9] Y.-C. Kang, S.-H. Ok, and S.-H. Kang, "A CT saturation detection algorithm," *IEEE Transactions on Power Delivery*, vol. 19, no. 1, pp. 78-85, Jan. 2004.
[10] S.-H. Kang, M.-S. Kim, S.-R. Nam *et al*., "A CT saturation detection algorithm based on wavelet transformation," in *Proceedings of 12th IET International Conference on Developments in Power System Protection*, Copenhagen, Denmark, Mar.-Apr. 2014, pp. 1-7.
[11] J. Ma, X. Gao, Z. Wang *et al*., "A new adaptive method to identify TA saturation using grille fractal," *Canadian Journal of Electrical and Computer Engineering*, vol. 36, no. 4, pp. 152-157, Aug. 2013.
[12] S. Biswal and M. Biswal, "Algorithm for CT saturation detection with the presence of noise," in *Proceedings of 4th International Conference on Electrical Energy Systems (ICEES)*, Chennai, India, Feb. 2018, pp. 248-251.
[13] A. Hooshyar, M. Sanaye-Pasand, and E. F. El-Saadany, "CT saturation detection based on waveshape properties of current difference functions," *IEEE Transactions on Power Delivery*, vol. 28, no. 4, pp. 2254-2263, Oct. 2013.
[14] T. Ji, Q. Wu, W. Tang *et al*., "A morphological scheme for the correction of CT saturation waveforms," in *Proceedings of 2011 IEEE PES General Meeting*, Detroit, USA, Jul. 2011, pp. 1-7.
[15] S. R. Mohantya, V. R. Pandi, B. K. Panigrahi *et al*., "Performance evaluation of distance relay with CT saturation," *Applied Soft Computing*, vol. 11, no. 8, pp. 4789-4797, Dec. 2011.
[16] E. M. Esmail, N. I. Elkalashy, T. A. Kawady *et al.,* "Detection of partial saturation and waveform compensation of current transformers," *IEEE Transactions on Power Delivery*, vol. 30, no. 3, pp. 1620-1622, Jun. 2015.
[17] A. Bagheri, M. Allahbakhshi, D. Behi *et al*., "Utilizing Rogowski coil for saturation detection and compensation in iron core current transformer," in *Proceedings of 25th Iranian Conference on Electrical Engineering (ICEE)*, Tehran, Iran, May 2017, pp. 1066-1071.
[18] B. Kasztenny and I. Voloh, "Application of distance and line current differential relays in breaker-and-a-half configurations," in *Proceedings of IEEE/PES Transmission and Distribution Conference and Exhibition*, Dallas, USA, May 2006, pp. 1-8.
[19] ABB. (2011, Feb.). Line distance protection REL650 technical manual. [Online]. Available: https://library. abb. com/share? cid=9AAC3030 1058
[20] Y. Yuan, Y. Lu, Z. Liu *et al*., "A fast filter algorithm of short data window based on phase analysis," *Automation of Electric Power Systems*, vol. 28, no. 3, pp. 58-63, Feb. 2004.
[21] Y. Sun, Z. Zhang, Y. Shi *et al*., "The short-window integral method for calculating fundamental component from fault transient signalsin power systems," *Automation of Electric Power Systems*, vol. 24, no. 1, pp. 30-33, Jan. 2000.
[22] W. Liu, Y. Pan, Y. Wang *et al*., "Effect of CT transient characteristics on transfer of inrush," *The Journal of Engineering*, vol. 2019, no. 16, pp. 3062-3066, Apr. 2019.
[23] N. Farshid, K. Zahra, F. Ebrahim *et al*., "Fast detection and compensation of current transformer saturation using extended Kalman filter," *IEEE Transactions on Power Delivery*, vol. 34, no. 3, pp. 1087-1097, Jun. 2019.
[24] A. Hooshyar and M. Sanaye-Pasand, "Accurate measurement of fault currents contaminated with decaying DC offset and CT saturation," *IEEE Transactions on Power Delivery*, vol. 27, no. 2, pp. 773-783, Apr. 2012.

Yuping Zheng received the B.Sc. degree from Hefei University of Technology, Hefei, Anhui, in 1983. He received the M.Sc. degree from Nanjing Automation Research Institute, Nanjing, China, in 1986, and the Ph.D. degree from Wuhan University, Wuhan, Hubei, in 2004. His research interests include relay protection and control of AC/DC hybrid power system.

Tonghua Wu received the B.Sc. degree from Hefei University of Technology, Hefei, China, in 1999, the M.Sc. degree from State Grid Electric Power Research Institute, Nanjing, China, in 2005. He is currently pursuing the Ph.D. degree of automation of electric power systems at Hohai University, Nanjing, China. His research interests include relay protection and control of AC/DC hybrid power system.

Feng Hong received the B.Sc. and M.Sc. degrees from Hohai University, Nanjing, China, in 2005 and 2011, respectively. His research interests include relay protection and control of AC/DC hybrid power system.

Gang Yao received the B.Sc. degree from Southeast University, Nanjing, China, in 2007, the master degree from State Grid Electric Power Research Institute, Nanjing, China, in 2010. His research interests include relay protection and control of AC/DC hybrid power system.

Jimin Chai received the B.Sc. degree from Xi'an Jiaotong University, Xi'an, China, in 2004. He is currently pursuing the Ph.D. degree of automation of electric power systems at Hohai University, Nanjing, China. His research interests include relay protection and control of power system.

Zhinong Wei received the B.Sc. degree from Hefei University of Technology, Hefei, China, in 1984, the M.Sc. degree from Southeast University, Nanjing, China, in 1987, and the Ph.D. degree from Hohai University, Nanjing, China, in 2004. His research interests include power system operation, analysis and control.